

# Nonlinear spectral blueshift in semiconductor optical amplifiers

A. E. BEDNYAKOVA,<sup>1,2,\*</sup> D. KHUDOZHITKOVA,<sup>1</sup> A. KOKHANOVSKIY,<sup>1</sup> AND S. K. TURITSYN<sup>1,3</sup>

<sup>1</sup>Novosibirsk State University, Novosibirsk 630090, Russia

<sup>2</sup>Institute of Computational Technologies, SB RAS, Novosibirsk 630090, Russia

<sup>3</sup>Aston Institute of Photonic Technologies, Aston University, Birmingham B4 7ET, UK

\*Corresponding author: anastasia.bednyakova@gmail.com

Received 28 July 2021; revised 24 August 2021; accepted 26 August 2021; posted 27 August 2021 (Doc. ID 438870); published 23 September 2021

**We demonstrate that spectral peak power of negatively chirped optical pulses can acquire a blueshift after amplification by a semiconductor optical amplifier. The central wavelength of a transform limited optical pulse translates over 20 nm towards a shorter wavelength after propagation in a single-mode fiber and semiconductor optical amplifier. A chirped Gaussian pulse with full width at half maximum 1 ps and dimensionless chirp parameter  $C = -20$  can be blueshifted by 5 THz.** © 2021 Optical Society of America

<https://doi.org/10.1364/OL.438870>

In the seminal paper [1], Mitschke and Mollenauer discovered a continuous shift in the optical frequency of a soliton pulse propagating down the optical fiber. This is a manifestation of the nonlinear phenomenon caused by a Raman-induced energy spectral transfer from the lower to higher wavelengths (redshift). Gordon in [2] introduced a theory of the Raman self-frequency shift for a pulse propagating in optical fibers. A possibility to shift the central frequency of the optical pulse (soliton) to the red part of the spectrum in a controllable manner paved the way for a variety of practical applications including frequency converters and spectrally tunable optical pulsed sources. The key attractive feature of the Raman soliton self-frequency shift for applications is a possibility of wavelength conversion to the spectral intervals that are not covered by easily available light sources. Due to the generic nature of the Raman effect, a spectral redshift is nowadays a well-established practical technique. However, there is no comparable easily implementable general method to produce blueshift of the spectral peak of radiation.

Note that stimulated Stokes Raman scattering is always accompanied by anti-Stokes Raman scattering, which produces waves at shorter wavelengths (or higher frequencies). However, the efficiency of coherent anti-Stokes scattering is typically much lower compared to the non-spontaneous Raman process, which has a dominant effect in a variety of conventional materials. Anti-Stokes Raman scattering can be enhanced in waveguides [3] and through special designs of such wavelength converters (for advances in this field, see, e.g., a recent review [4] and references therein).

Blueshift of radiation can be achieved by using higher-order harmonics generation. Second and third harmonics are routinely used for light upconversion. High-order harmonics [5,6] (more than 25 harmonics) can be used for generation of extreme ultraviolet radiation. Parametric processes supported by Kerr nonlinearity, more specifically, four-wave mixing and cross-phase modulation, are successfully used for light upconversion [7–10]. In [11–13], the effect of spectral blueshift was studied and experimentally demonstrated. It is shown in [12,13] that the photoionization effect (when the intensity of solitons is slightly above the photoionization threshold) in a hollow-core photonic crystal fiber filled with a Raman-inactive noble gas produces a constant acceleration of solitons in the time domain with a continuous shift to higher frequencies. Among the key challenges of existing upconversion techniques is efficiency of such processes. In this Letter, we propose a relatively simple alternative possibility to achieve blueshift of optical pulses using a commercially available semiconductor optical amplifier (SOA).

The SOA is an important practical device developed for optical communication systems. It exhibits many attractive characteristics, including compactness, low power consumption, and wide gain bandwidth. Beyond direct applications as an amplifier, SOA is used in all-optical signal processing, and applications such as radio over fiber, modulators, and emerging neuromorphic photonics [7,14–16]. SOA transformed the field of nonlinear optical techniques for data processing at high speed, and it can operate at 100 Gb/s and higher [14]. SOA is also an example of a physical system with interesting nonlinear properties, often considered by engineers as a drawback and undesirable feature of the device.

The transmission characteristics of the SOA are described by a conventional rate equation for carrier density and a linear relationship between the carrier density and induced complex susceptibility [17]. Neglecting the dispersion within the SOA, the transient response is modeled [17] by a time-dependent gain  $h(t)$  and a linewidth enhancement factor  $\alpha_H$  as

$$A_{\text{out}}(t) = \exp[(1 - i\alpha_H)h(t)/2]A_{\text{in}}(t),$$

$$\frac{dh}{dt} = -\frac{h - h_0}{T_{\text{SOA}}} - \frac{|A_{\text{in}}(t)|^2}{E_{\text{sat}}}[\exp(h) - 1], \quad (1)$$

where  $A_{\text{in}}(t)$  and  $A_{\text{out}}(t)$  are, respectively, the input and output optical fields,  $h_0$  is related to the small signal gain  $G_0 = \exp(h_0)$ ,  $T_{\text{SOA}}$  is the gain recovery time,  $E_{\text{sat}}$  is a characteristic saturation energy that defines the SOA saturation power  $P_{\text{sat}} = E_{\text{sat}}/T_{\text{SOA}}$ , and  $\alpha_H$  is the so-called Henry linewidth enhancement factor. We consider without loss of generality the typical parameters  $\alpha_H = 5$ ,  $E_{\text{sat}} = 8$  pJ, and  $T_{\text{SOA}} = 200$  ps for all numerical modeling hereinafter.

We examine here application of the SOA as a nonlinear device that transforms the input signal  $A_{\text{in}}(t)$  into the field  $A_{\text{out}}(t) = \sqrt{P_{\text{out}}} \times \exp[i\phi_{\text{out}}]$ . Equation (1) cannot be solved analytically; therefore, we examine numerically the transformation of the initially chirped Gaussian pulse having the form  $A_{\text{in}}(t) = \sqrt{P_0} \exp[-\frac{1+iC}{2} \frac{t^2}{\tau^2}]$ .

In the limit  $\tau \ll T_{\text{SOA}}$ , we can use a well-known approximated solution to Eq. (1) [17]:

$$h(t) = -\ln \left[ 1 - \left( 1 - \frac{1}{G_0} \right) \exp \left( -\frac{U_{\text{in}}(t)}{E_{\text{sat}}} \right) \right],$$

where  $U_{\text{in}}(t) = \int_{-\infty}^t P_{\text{in}}(s) ds$ . In this limit, the output pulse power and the instantaneous frequency  $\Omega_{\text{out}} = d\phi_{\text{out}}/dt$  are [17]

$$P_{\text{out}}(t) = P_{\text{in}}(t) \exp[h(t)] = \frac{E_{\text{sat}} G_0}{G_0 - 1} \times \frac{dh}{dt}, \quad (2)$$

$$\frac{d\phi_{\text{out}}}{dt} + C \frac{t}{\tau^2} = \frac{\alpha_H}{2} \frac{dh}{dt} = -\frac{\alpha_H(G_0 - 1)}{2G_0 E_{\text{sat}}} \times P_{\text{out}}(t). \quad (3)$$

Input signal (chirped Gaussian pulse) is nonlinearly transformed by SOA. This functional transformation depends on the input signal parameters ( $\tau$ ,  $P_{\text{in}}$ ,  $C$ ) and SOA parameters (gain  $G_0$  and Henry factor  $\alpha_H$ ). This makes challenging full characterization of SOA-based nonlinear transformation. Though the output pulse does not have a Gaussian shape after SOA transformation, we can highlight several important features of input–output mapping. Our focus will be on the output pulse spectrum. More specifically, we examine a possibility of the control of the spectral shift of the peak of the pulse spectrum by varying input field characteristics.

The nonlinear transformation implemented with SOA is illustrated in Figs. 1–3.

Figure 1 shows a shift of the central wavelength (peak of the spectral power distribution) of the initially chirped Gaussian pulse with 1 ps duration and varying peak powers. For a positive and small negative chirp  $C > -5$ , the pulse spectrum shifts to the red side, having a stationary point in the vicinity of  $C = -5$  [white line in Fig. 1(a)]. This is a well-known and studied effect [17]. If the absolute value of chirp increases  $C < -5$ , blueshift takes place.

Transformation of temporal shape, spectrum, and instant frequency, corresponding to negative chirp  $C = -20$ , is shown in Fig. 2. Peak power growth leads to an increase in the spectrum shift to the blue side due to the influence of the SPM-induced term in Eq. (3). The temporal pulse shift is also getting larger. Figure 2(c) shows SPM-induced frequency chirp imposed on the pulse as it propagates through the amplifier.

Visualization of nonlinear pulse transformation in spectral and temporal domains can be done simultaneously with a spectrogram. Figure 3 depicts spectrograms, corresponding to several values of the input chirp. Arrows point out the

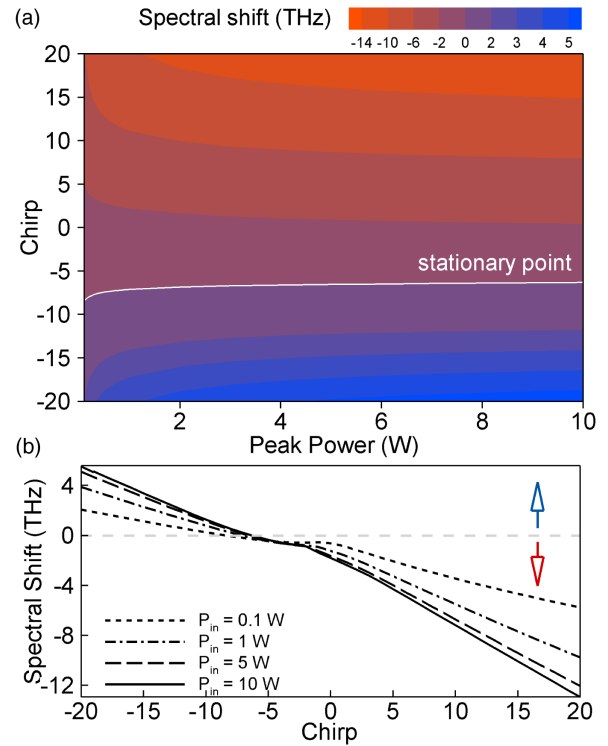


**Fig. 1.** (a) Spectral shift of the amplified pulse presented in the plane of the peak power and chirp of the initial pulse. Here  $T_{\text{FWHM}}^{\text{in}} = 1$  ps,  $G_0 = 30$  dB. (b) Spectral shift of the maximum of the pulse spectrum after SOA for varying input peak powers.

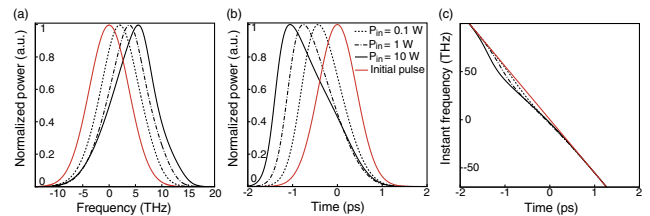


**Fig. 2.** (a) Pulse spectrum, (b) temporal shape, and (c) instantaneous frequency at SOA input (red line) and output.  $T_{\text{FWHM}}^{\text{in}} = 1$  ps,  $G_0 = 30$  dB,  $C = -20$ .

direction of the pulse peak shift in the time–frequency space. Note that pulse shape  $P_{\text{out}}(t)$  and its temporal shift do not depend on the initial chirp [see Eq. (2)], so the  $x$  coordinate of the end of the arrow does not change. The maximum of the instantaneous frequency is reached at the same time as the maximum of output pulse intensity, forming a distinct peak in two-dimensional space, whose  $y$  coordinate corresponds to a spectral shift. Direction and angle of arrows rotation in Fig. 3 are determined by a balance between two terms in the following expression defining the maximum of instantaneous frequency  $\Delta\Omega_{\text{max}} = \max(d\phi_{\text{out}}/dt)$ :

$$\Delta\Omega_{\text{max}} = -C \frac{t_p}{\tau^2} - \frac{\alpha_H(G_0 - 1)}{2G_0 E_{\text{sat}}} \times P_{\text{out}}(t_p), \quad (4)$$

where  $t_p < 0$  is a position of pulse maximum in time. The first term describes the input-pulse chirp and the second term additive SPM-induced chirp, which does not depend on the initial chirp. For small positive chirp  $C \sim 5$ , two terms are equal

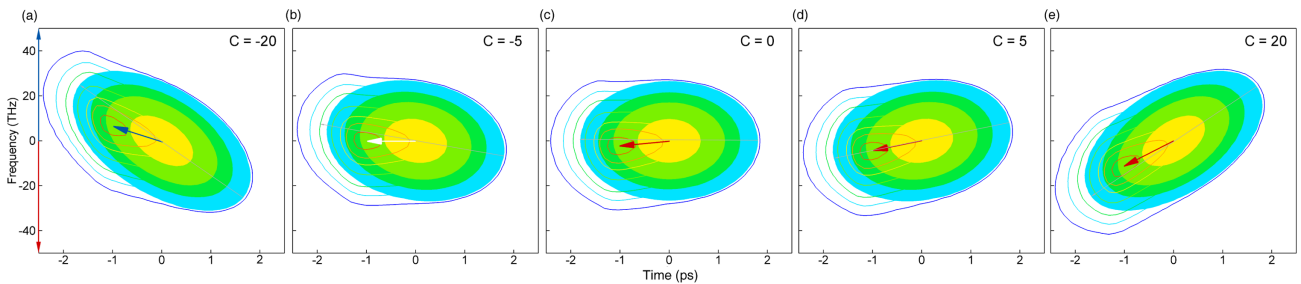


**Fig. 3.** Pulse spectrogram at SOA input (filled ovals) and output (colored lines) corresponding to different values of chirp parameter. Blue arrow depicts blueshift of the central wavelength of an optical pulse, and red arrows redshift.

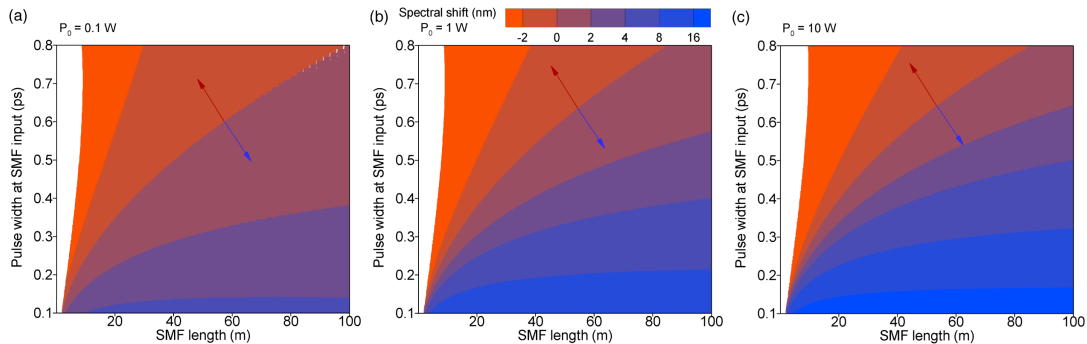


**Fig. 4.** Spectral shift of the initially unchirped Gaussian pulse with 0.1–10 W peak power after propagation in SMF and subsequent amplification in SOA. Pulse width at SOA input exceeds 1 ps.

[Fig. 3(d)], and the arrow does not rotate in relation to the initial phase slope. For a zero or negative chirp, arrow rotation is counterclockwise [Figs. 3(a)–3(c)]. For a positive chirp, rotation becomes clockwise, leading to a well-known redshift of the pulse.

Then we examined whether it is possible to realize the blueshift in a simple experimental setup consisting of laser pulse source operating at 1550 nm and single-mode fiber (SMF) up to 100 m long. As a source of ultrashort pulses, we have used a mode-locked fiber laser based on the nonlinear polarization evolution effect. The cavity comprised elements based on SMF-28 fiber; therefore, cavity chromatic dispersion was anomalous. The laser generated nearly Fourier-limited pulses at a repetition rate of 14.51 MHz and up to 10 pJ energy. A pulse acquires a negative chirp during propagation in SMF-28 fiber, and passes through SOA (Thorlabs BOA1004P), carrying out the nonlinear pulse transform. The pumping current of the SOA was varied from 0 to 150 mA. At higher values of current, we observed significant amplification of broadband background optical noise. Output radiation at the SOA output was measured by an optical spectrum analyzer (Yokogawa AQ6370D) with spectral resolution of 0.2 nm. To model pulse propagation in SMF, we used the generalized nonlinear Schrödinger equation, which takes into account Kerr nonlinearity ( $\gamma = 1.1 \text{ W}^{-1} \text{ km}^{-1}$ ), second- and third-order dispersion ( $\beta_2 = -20 \text{ ps}^2/\text{km}$ ,  $\beta_3 = 0.132 \text{ ps}^3/\text{km}$ ), and Raman gain. The equation was solved by the standard split-step Fourier-transform method implemented in C++, in which the integration at a nonlinear step was performed using the Runge–Kutta method. The temporal window was equal to 100 ps with  $2^{15}$  points in the grid. The results of simulations are shown in Fig. 4. It should be noted that only the region corresponding to a

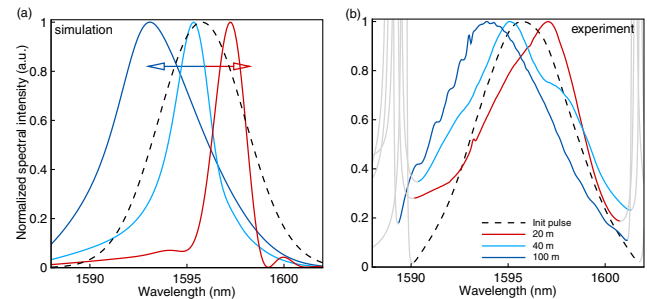


**Fig. 5.** Normalized pulse spectra after propagation in SMFs 20, 40, and 100 m long and consequent amplification in SOA in (a) simulation and (b) experiment.  $G_0 = 27 \text{ dB}$ . Experimental spectra feature Kelly's sidebands shown by gray lines.

pulse duration of more than 1 ps at SOA input (after dispersive broadening in SMF) is shown in the figures. Within this region, the model of SOA (1) remains valid. Even for the smallest considered peak power  $P_0 = 0.1 \text{ W}$  of the initial pulse, blueshift is possible if pulse duration lies below 0.8 ps. If we increase peak power at SMF input, blueshift could exceed 20 nm. Figure 5 depicts a comparison of calculated and experimental spectra. A laser pulse with 10 W peak power, 0.8 ps duration, and small negative chirp  $C = -0.5$  propagates through 20, 40, and 100 m of SMF and then amplifies in SOA. Both experiment and simulation demonstrate redshift for 20 m long fiber and blueshift for 40 and 100 m long fiber. Calculated spectral shapes qualitatively agree with the measured ones.

Therefore, even in such a simple scheme, the central wavelength of subpicosecond pulses could be shifted to a blue part of the spectrum. Basically, we can use this physical effect to expand

the blue part of the spectrum for any spectral interval covered by semiconductor optical amplifiers in pulsed optical source applications. We point out that the observed effect can find applications beyond simple wavelength converters and optical sources. One of the potential emerging applications where this effect can be useful is the development of neuromorphic computing photonic devices. More specifically, our findings potentially might be useful in the design of SOA-based optical neuromorphic devices operating with signal in the spectral domain, either for masking or in the output layer for reservoir computing systems; see, e.g., [18–21].

In conclusion, we demonstrated that optical pulses with an appropriate initial chirp can undergo a nonlinear spectral blueshift, opposite the Raman-induced redshift, when they are amplified by a semiconductor amplifier. The results offer new opportunities for manipulation and control of the central frequency of optical pulses.

**Funding.** Russian Science Support Foundation (21-42-04401).

**Disclosures.** The authors declare no conflicts of interest.

**Data Availability.** Data underlying the results presented in this paper are not publicly available at this time but may be obtained from the authors upon reasonable request.

## REFERENCES

1. F. M. Mitschke and L. F. Mollenauer, *Opt. Lett.* **11**, 659 (1986).
2. J. P. Gordon, *Opt. Lett.* **11**, 662 (1986).
3. R. Claps, V. Raghunathan, D. Dimitropoulos, and B. Jalali, *Opt. Express* **11**, 2862 (2003).
4. N. Vermeulen, C. Debaes, and H. Thienpont, *Laser Photon. Rev.* **4**, 656 (2010).
5. I. Pupeza, S. Holzberger, T. Eidam, H. Carstens, D. Esser, J. Weitenberg, P. Rußbüldt, J. Rauschenberger, J. Limpert, T. Udem, A. Tünnermann, T. W. Hänsch, A. Apolonski, F. Krausz, A. V. E. Sokolov, D. R. Walker, D. D. Yavuz, G. Y. Yin, and S. E. Harris, *Nat. Photon.* **7**, 608 (2013).
6. A. V. Sokolov, D. R. Walker, D. D. Yavuz, G. Y. Yin, and S. E. Harris, *Phys. Rev. Lett.* **85**, 562 (2000).
7. R. J. Manning, A. D. Ellis, A. J. Poustie, and K. J. Blow, *J. Opt. Soc. Am. B* **14**, 3204 (1997).
8. T. Durhuus, B. Mikkelsen, C. Joergensen, S. Lykke Danielsen, and K. Stubkjaer, *J. Lightwave Technol.* **14**, 942 (1996).
9. M. Matsuura, O. Raz, F. Gomez-Agis, N. Calabretta, and H. J. S. Dorren, *Opt. Express* **19**, B551 (2011).
10. M. Matsuura, O. Raz, F. Gomez-Agis, N. Calabretta, and H. J. S. Dorren, *Opt. Lett.* **38**, 238 (2013).
11. V. N. Serkin and V. A. Vysloukh, "Femtosecond spectral tunneling effect in fibers," in *Conference on Lasers and Electro-Optics (Optical Society of America, 1993)*, p. CFD7.
12. S. P. Stark, A. Podlipensky, and P. S. J. Russell, *Phys. Rev. Lett.* **106**, 083903 (2011).
13. M. F. Saleh, W. Chang, P. Hölzer, A. Nazarkin, J. C. Travers, N. Y. Joly, P. S. J. Russell, and F. Biancalana, *Phys. Rev. Lett.* **107**, 203902 (2011).
14. D. Cotter, R. J. Manning, K. J. Blow, A. D. Ellis, A. E. Kelly, D. Nasset, I. D. Phillips, A. J. Poustie, and D. C. Rogers, *Science* **286**, 1523 (1999).
15. J. Mork and T. W. Berg, *Opt. Photon. News* **14**, 42 (2003).
16. D. Brunner, B. Penkovsky, B. A. Marquez, M. Jacquot, I. Fischer, and L. Larger, *J. Appl. Phys.* **124**, 152004 (2018).
17. G. Agrawal and N. Olsson, *IEEE J. Quantum Electron.* **25**, 2297 (1989).
18. A. N. Tait, J. Chang, B. J. Shastri, M. A. Nahmias, and P. R. Prucnal, *Opt. Express* **23**, 12758 (2015).
19. L. Butschek, A. Akrouf, E. Dimitriadou, M. Haelterman, and S. Massar, "Frequency-multiplexed photonic reservoir computing," in *Frontiers in Optics + Laser Science APS/DLS (Optical Society of America, 2019)*, p. JW3A.122.
20. T. Hashimoto, M. Nakajima, and K. Tanaka, *Commun. Phys.* **4**, 1 (2021).
21. M. Sorokina, *J. Phys.: Photon.* **3**, 014002 (2020).